# A New Framework for the Integrative Analytics of Intravascular Ultrasound and Optical Coherence Tomography Images

**CHENXI HUANG[1], YUAN XIE[1], YISHA LAN[1], YONGTAO HAO[1], FEI CHEN[2], YONGQIANG CHENG[3], AND YONGHONG PENG[4], (Member, IEEE)**

[1]Department of Computer Science and Technology, Tongji University, Shanghai 201804, China
[2]Department of Cardiology, Shanghai Tongji Hospital, Tongji University, Shanghai 200065, China
[3]School of Engineering and Computer Science, University of Hull, Hull HU6 7RX, U.K.
[4]Faculty of Computer Science, University of Sunderland, St Peter Campus, Sunderland SR6 0DD, U.K.

Corresponding author: Yongtao Hao (hao0yt@163.com)

**ABSTRACT** The integrative analysis of multimodal medical images plays an important role in the diagnosis of coronary artery disease by providing additional comprehensive information that cannot be found in an individual source image. Intravascular ultrasound (IVUS) and optical coherence tomography (IV-OCT) are two imaging modalities that have been widely used in the medical practice for the assessment of arterial health and the detection of vascular lumen lesions. IV-OCT has a high resolution and poor penetration, while IVUS has a low resolution and high detection depth. This paper proposes a new approach for the fusion of intravascular ultrasound and optical coherence tomography pullbacks to significantly improve the use of those two types of medical images. It also presents a new two-phase multimodal fusion framework using a coarse-to-fine registration and a wavelet fusion method. In the coarse-registration process, we define a set of new feature points to match the IVUS image and IV-OCT image. Then, the improved quality image is obtained based on the integration of the mutual information of two types of images. Finally, the matched registered images are fused with an approach based on the new proposed wavelet algorithm. The experimental results demonstrate the performance of the proposed new approach for significantly enhancing both the precision and computational stability. The proposed approach is shown to be promising for providing additional information to enhance the diagnosis and enable a deeper understanding of atherosclerosis.

**INDEX TERMS** Intravascular ultrasound (IVUS), optical coherence tomography (OCT), wavelet fusion, mutual information registration, feature registration.

## I. INTRODUCTION

Coronary atherosclerosis is the main cause of death worldwide and is becoming a major health problem [1]–[3]. Atherosclerosis appears to have a much higher death rate every year compared to other diseases [4]. Assessment of human coronary atherosclerosis by histology is the standard approach at present. However, histology remains restricted to postmortem conditions other than *in vivo*. Medical imaging is an effective way to help doctors make a more accurate diagnosis of cardiovascular disease. Two image technologies are predominantly used in research and the clinical setting, namely, intravascular ultrasound (IVUS) [5] and optical coherence tomography (OCT) [6].

The principle of IVUS is similar to the traditional B ultrasound, with differences in that IVUS makes smaller ultrasonic probes so that they can be put inside the vascular lumen to observe its interior conditions with a 360-degree view. The resolution is $100\mu m$, the depth of penetration can reach $4{\sim}8$ mm, and the scanning range is $10{\sim}15$ mm. Because of the reflection phenomenon of the ultrasonic wave being used, it was beneficial to display the deep structures. Nonetheless, IVUS is limited when distinguishing fine structures.

Different from IVUS, the OCT is a relatively new technology, used for clinical applications since 2005. IV-OCT uses infrared instead of an ultrasonic wave. OCT has a higher value of resolution, and its axial resolution is in the range

of 4-10$\mu$m, which is 10-20 times that of IVUS (approximately 70-100$\mu$m). However, its ability to penetrate tissue is obviously less than IVUS, which has a maximum of about 2 mm, with a scanning range of 7 mm.

Considering the fundamental differences in imaging physics leading to different information obtained by IVUS and OCT, the combination of these two imaging modalities would take advantage of the high spatial resolution of IV-OCT and the high penetration depth of IVUS [7], [8]. This offers a new possibility for gaining more comprehensive information in the lumen vessel, thus increasing the specificity when detecting vulnerable plaques for diagnosing. On-line hybrid imaging and off-line image fusion are two approaches for the implementation of image fusion. For the former, the integrated intravascular imaging probes combining IVUS with IV-OCT have been developed in the literature. For example, a flexible 4F (1.33-mm diameter), 1.3-m-long hybrid imaging catheter containing the ability to acquire coplanar IVUS simultaneously and OCT imaging data from coronary arteries was proposed in [9]. In [10], a miniature integrated optical coherence tomography and ultrasound probing system for intravascular imaging applications was developed. However, this technology is not in widespread use because of its security. Further research is needed to put this integrated technology into clinical practice.

An increasing number of studies have been conducted for the off-line co-registration and fusion of IVUS and IV-OCT cross-sections that are acquired on the same vessel segment. The generated multimodal image might improve the assessment of coronary atherosclerosis in a new way. For example, a registration and fusion method for IV-OCT and IVUS images acquired on the same vessel segment was proposed in [11]. The limitation of this method is that it is difficult to extract the boundary between the intima and stent struts causing failure of registration. In Pauly *et al.*, [12] the semi-automatic fusion of intravascular ultrasound and optical coherence tomography based on the characterization of the lumen shape by a set of Gabor Jet features was presented. A computer-assisted image fusion of IVUS and OCT by a two-phase registration was put forward in image processing in [13]. It can take advantage of the deep penetration of IVUS and high resolution of OCT for the imaging of a plaque. Nonetheless, it requires prior matched frames with discernable features that must be provided manually. Recently, a framework for the co-registration of intravascular ultrasound and optical coherence tomography coronary artery pullbacks was proposed in [14]. That study implements a useful framework through dynamic time warping and dynamic programming algorithms. However, it showed poor performance once the artery and plaque had changed significantly between timepoints.

This study developed a new integrative analytics framework for the fusion of intravascular ultrasound and optical coherence tomography images that could enhance the precision of registration and provide a new way to visualize the details after fusing for assisting in diagnosis. In this paper, we present a new approach for coarse-to-fine registration using feature points and the integration of mutual information extracted from IVUS and IV-OCT, respectively. We compare the output of the different algorithms including the feature-based method and gray mutual information registration, which have been widely used in the literature. The experimental results demonstrate the validity and performance of the proposed framework.

The remaining part of the paper is organized as follows: the methodology we use in image registration and fusion of IVUS and IV-OCT is introduced in Section II. The experimental results and discussion are given in Section III. Finally, we conclude this paper and discuss the future work in Section IV.

## II. METHODOLOGY

The proposed framework for the fusion of intravascular ultrasound and optical coherence tomography is presented in Fig. 1, which consists of a coarse-registration, a fine-registration and an image fusion. Firstly, the feature points are extracted from the original IVUS and OCT images including the contour points, side branches and stent struts for the image registration. Secondly, the mutual information is used to define the independence of variables between the two images [15]. To achieve higher registration, this paper presents a coarse-to-fine image registration method based on the feature points and the gray mutual information registration. Thirdly, different fusion algorithms including the wavelet fusion [16], IHS fusion [17], PCA fusion [18] and weighted fusion [19] are investigated to find the optimal algorithm. Finally, the fused image is obtained by using the improved wavelet fusion.

### A. FEATURE POINTS EXTRACTION

Feature points are the part of the information extracted from the IVUS and IV-OCT necessary to gain a more detailed understanding of the images. Commonly used features in medical images include corresponding points, and boundaries [20]. In this study, we extract the feature points for the following image registrations. According to the characteristics of intravascular images, we choose three kinds of points to form the feature points including the lumen boundary, the side branches, and the stent struts. The spatial filter is used to reduce the speckle noises, which are common in medical images. By imposing spatial continuity between adjacent frames and focusing on inter-frame point-point connectivity, the boundary was defined [21]. The extracted boundaries are regarded as the feature points. The side branch normally appears as a cavity when the vessel being imaged bifurcates in intravascular images.

Two steps are proposed to define the side branch: (1) the distance profile along the single frame is computed to detect the candidate region. When the profile of the distance has two peaks, it represents that the side branch is contained. (2) The gradient of the width of the candidate region is computed. The side branch can be identified if the gradient value exceeds the threshold [22].
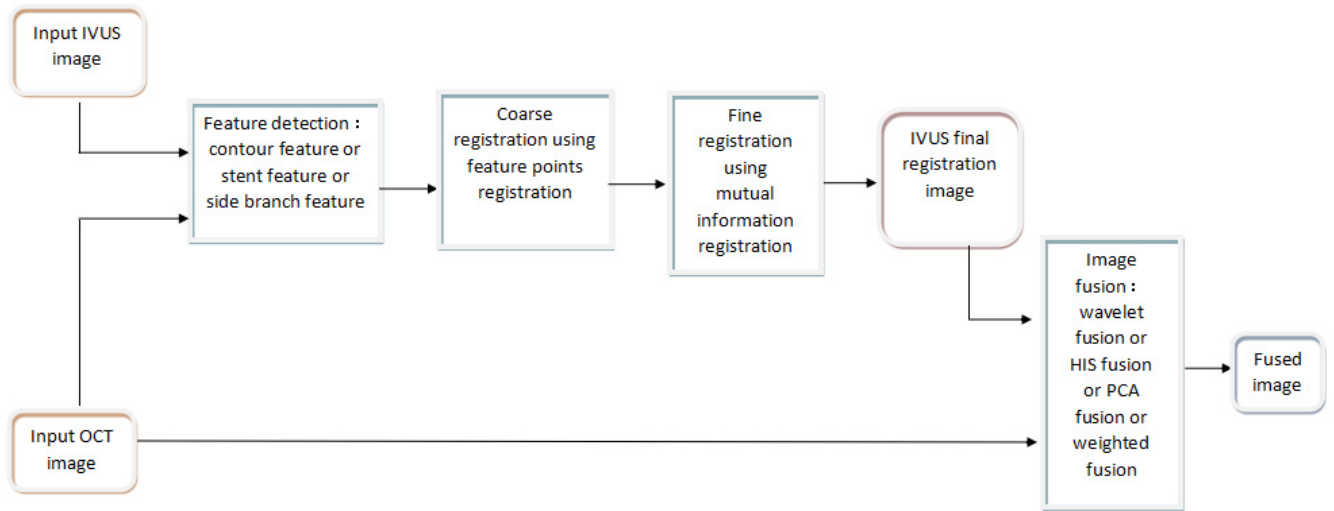
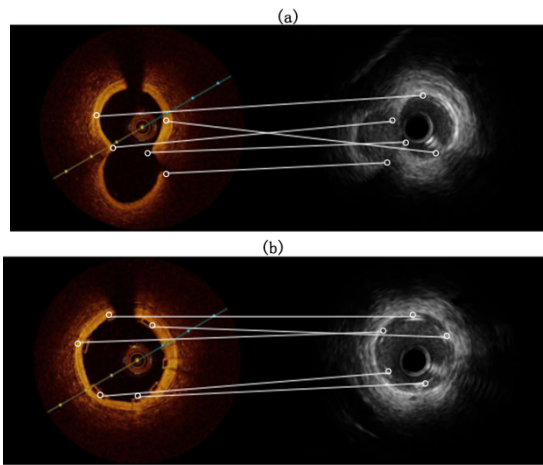**FIGURE 1.** The proposed framework for image fusion.



**FIGURE 2.** Feature points of different original images. (a) An original image with side branch; (b) an original image with a stent.

The stent struts are the special and important landmarks for registration in intravascular images. In IV-OCT images, a bioresorbable stent strut usually appears as a box-shape with no trailing shadow. The seed points in the middle of the BVS struts by scan-line were selected. The improved region growing algorithm was used to automatically detect the black core region [23]. In IVUS images, the cascade of GentleBoost classifiers was employed to detect the stent struts using structural features [24].

### B. CASCADED FEATURE POINTS AND MUTUAL INFORMATION REGISTRATION FOR IVUS AND IV-OCT IMAGES

The methods for medical image registration consist of two categories: feature-based and intensity-based methods. The feature-based methods need to pre-define the features, while intensity-based methods use the gray information of the images directly [17], [18]. In feature-based registration, when

the pairs of matching points are obtained, the affine transformation between the reference image and input image can be defined by Eq. (1)

$$\begin{bmatrix} x_{A,i} \\ y_{A,i} \end{bmatrix} = s \begin{bmatrix} \cos\varphi & \sin\varphi \\ -\sin\varphi & \cos\varphi \end{bmatrix} \begin{bmatrix} x_{B,i} \\ y_{B,i} \end{bmatrix} + \begin{bmatrix} \Delta x \\ \Delta y \end{bmatrix} \quad (1)$$

where $s$ is the gain factor, $\psi$ is the rotation angle, $\Delta x$, $\Delta y$ represents translation in the direction of $x$, $y$, $(x_{A,i}, y_{A,i})$ represents the feature point in the input image, and $(x_{B,i}, y_{B,i})$ represents the feature point in the reference image. The transform parameters above can be obtained through the method of least mean square error and are mathematically expressed as follows:

$$\hat{s} = \frac{\sum\limits_{i=1}^{M}\sum\limits_{j=1}^{M}\sqrt{(x_{A,i}-x_{A,j})^2+(y_{A,i}-y_{A,j})^2}}{\sum\limits_{i=1}^{M}\sum\limits_{j=1}^{M}\sqrt{(x_{B,i}-x_{B,j})^2+(y_{B,i}-y_{B,j})^2}} \quad (2)$$

$$\hat{\varphi} = \frac{1}{M-1}\sum\limits_{i=1}^{M}\sum\limits_{j=1}^{M}\left[\tan^{-1}\left(\frac{y_{A,i}-y_{A,j}}{x_{A,i}-x_{A,j}}\right)\right.$$
$$\left. -\tan^{-1}\left(\frac{y_{B,i}-y_{B,j}}{x_{B,i}-x_{B,j}}\right)\right] \quad (3)$$

$$\begin{bmatrix} \Delta\hat{x} \\ \Delta\hat{y} \end{bmatrix} = \frac{1}{N}\sum\limits_{i=1}^{M}\left\{\begin{bmatrix} x_{B,j} \\ y_{B,j} \end{bmatrix} - \hat{s}\begin{bmatrix} \cos\varphi & \sin\varphi \\ -\sin\varphi & \cos\varphi \end{bmatrix}\begin{bmatrix} x_{A,j} \\ y_{A,j} \end{bmatrix}\right\} \quad (4)$$

However, the feature-based method has some limitations. First, the process of image feature detection is sensitive to noise, so there are some errors in the positions of feature points. Then, it is difficult to match feature point pairs in two images accurately. Second, the number of feature points extracted from two images is unequal, which causes difficulty in determining the corresponding relationship between them [25].

Max-relativity and maximum mutual information can be obtained in two images during registration. The image registration based on mutual information is a process that involves seeking a space transformation relation to achieve the maximum mutual information of two images. It can be described in three main steps. First, one image is used as a reference image and the other one as a floating image to define a unified coordinate system. In this way, a form of space transformation is obtained. Next, according to the coordinate transformation, points in the floating image are transformed to the coordinate system in the reference image. Then, gray-level interpolation for the points of non-integer coordination is carried out after transformation, and mutual information of the two images is calculated. Last, space transformation parameters making maximum mutual information are obtained by changing the values of the parameters constantly. However, the approach above has limitations, especially for intravascular images. First, it is sensitive to gray change and it bases the whole image on gray level information. So a large computational capacity and a low rate appear. Next, a gray feature of the image is only used when registering results in neglecting the influence of other image characteristics and the sensitivity to noise. Moreover, this approach has inferior stability and is easy to fall into local extremum, which results in the mismatching of images.

To achieve higher registration precision, a new coarse-to-fine registration method based on feature points and mutual information for medical image registration is proposed. This method (as shown in Algorithm 1) contains a coarse-registration and a fine-registration.

---

**Algorithm 1** The Proposed Image Registration Approach

BEGIN
Step 1: *Input:* The original image
Step 2: Mark feature points on the original image, including stent points and lateral branch points.
Step 3: Obtain the contour image through special treatment. Convert the rectangular coordinates into polar coordinated views and fill the upper half of the image contour with white. Meanwhile, fill the lower part with black. Then, the special processed contour image is generated by converting the polar coordinates again.
Step 4: Use marked feature points to register both the original and contour image based on feature points.
Step 5: Perform registration based on the gray scale on the contour image after the feature-based registration.
Step 6: The transform domain obtained from the gray level registration of outline drawing is applied to the original image after the feature-based registration, completing the gray registration indirectly.
Step 7: *Output:* The registered image
END

---

The proposed new method for image registration is shown in Fig. 3, which consists of six key steps based on the combination of feature points and gray mutual information.

(1) An IVUS image and an OCT image are input separately;
(2) The contour images of both IVUS and OCT are obtained through the process of contour detection;
(3) The features of the original IVUS and OCT images are detected, which contain side branch detection and stent struts detection;
(4) By matching feature points pairs, a feature-based coarse-registration is carried out that requires both original and contour IVUS images;
(5) A fine-registration based on mutual information for the OCT contour image is processed, and a fine-registration above is considered for IVUS contour coarse-registration;
(6) In the end, a registered image is obtained through the IVUS final registration.

## C. IMPROVED WAVELET TRANSFORMATION FUSION BASED ON IVUS AND IV-OCT IMAGES

The current image fusion methods are divided into two categories: one is to fuse source images in a spatial domain directly, and the other is to integrate source images in the transform domain. IHS transform and fusion has a shortage of spectral distortion in image fusion. The PCA Fusion Algorithm leads to fuzziness and imperfection of the image. Moreover, the weighted average fusion rule weakens the details of the image. It also decreases the contrast ratio of an image, which confuses the edges in the image to a certain extent. To overcome these drawbacks, wavelet fusion is used in this study.

In the proposed Algorithm-2, an image fusion is carried out for registered IVUS and IV-OCT images based on wavelet transformation.

---

**Algorithm 2** Wavelet Fusion Method

BEGIN
Step 1: Wavelet decomposition is carried out in medical image preparation fusion.
Step 2: Both high frequency (HF) and low frequency (LF) sub-images of each decomposition layer are obtained from Step 1.
Step 3: Use the LF and HF fusion rules to integrate the HF and LF wavelet coefficients on the associated decomposition layer.
Step 4: The Wavelet transform coefficients of different portions and/or bands are obtained with the fusion rule.
Step 5: Using the combined transform coefficients above, the fused image is reconstructed by performing an inverse wavelet transform.
END

---

As a mathematical tool that can detect local features in a signal process, the algorithm of image fusion based on wavelet transformation offers a better solution in the following aspects. Firstly, the decomposition of multi-resolution provides the information of images under different
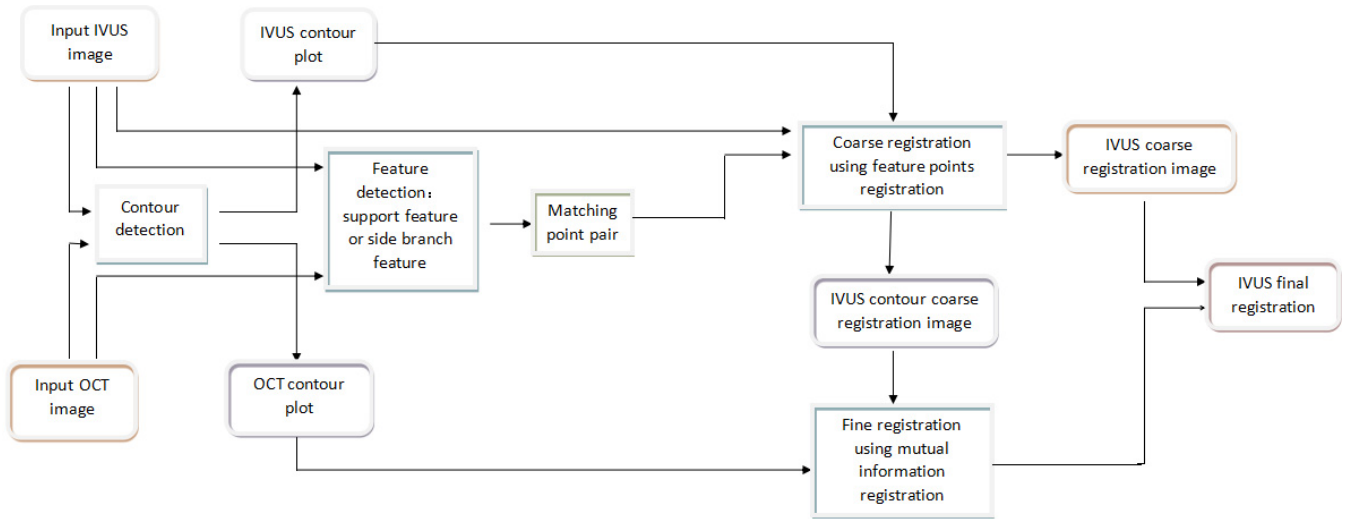
**FIGURE 3.** The proposed approach for image registration.

resolutions, and energies after transformation are mostly concentrated in low-frequency parts. Secondly, it can be used to decompose two-dimensional signals into different resolution levels. It can be ready to implement the algorithms in hardware as the wavelet decomposition and reconstruction can be calculated and recycled. Moreover, wavelet-based fusion provides a convenient way to extract detailed information and structural information of the original image. Last, it makes parallel processing and implementation easy.

Fig. 4 shows the procedure for the fusion of IVUS and OCT images based on wavelet transformation. Firstly, the discrete graphs of IVUS and OCT are obtained after wavelet decomposition. Multi-scale images are produced through fusion processing by using the LF and HF fusion rules, which are formulas of wavelet fusion. The combination of multi-scale images ahead creates a final fusion image in the end.

A flexible multi-resolution analysis of an image can be provided by Discrete Wavelet Transform (DWT), which implements a spatial-frequency decomposition. Suppose that a discrete signal is represented by f(t); the wavelet decomposition is then defined as

$$f(t) = \sum_{m,n} c_{m,n} \psi_{m,n}(t) \tag{5}$$

where $\psi_{m,n}(t) = 2^{-m/2} \psi[2^{-m}t - n]$ and $m$ and $n$ are integers. The wavelet decomposition algorithm of two-dimensional images is proposed through the Mallat algorithm of one-dimensional discrete wavelet transformation, by Eqs. (3) and (4):

$$
\begin{cases}
c_{j+1,m,n} = \sum_{k\in Z}\sum_{l\in Z} p(k-2m)p(l-2n)c_{j,k,l} \\
d^{\mathrm{v}}_{j+1,m,n} = \sum_{k\in Z}\sum_{l\in Z} p(k-2m)q(l-2n)c_{j,k,l} \\
d^{\mathrm{h}}_{j+1,m,n} = \sum_{k\in Z}\sum_{l\in Z} q(k-2m)p(l-2n)c_{j,k,l} \\
d^{\mathrm{d}}_{j+1,m,n} = \sum_{k\in Z}\sum_{l\in Z} q(k-2m)q(l-2n)c_{j,k,l}
\end{cases}
\tag{6}
$$

Moreover, the reconstruction algorithm is measured as

$$
\begin{aligned}
c_{j,m,n} = & \sum_{k\in Z}\sum_{l\in Z} p(m-2k)p(n-2l)c_{j,k,l} \\
& + \sum_{k\in Z}\sum_{l\in Z} p(m-2k)q(n-2l)d^{\mathrm{v}}_{j+1,k,l} \\
& + \sum_{k\in Z}\sum_{l\in Z} q(m-2k)p(n-2l)d^{\mathrm{h}}_{j+1,k,l} \\
& + \sum_{k\in Z}\sum_{l\in Z} q(m-2k)q(n-2l)d^{\mathrm{d}}_{j+1,k,l}
\end{aligned}
\tag{7}
$$

where $C_{j+1}$ represents the LF wavelet coefficient of the decomposition image of the $j+1$th layer; $C_j$ represents the LF wavelet coefficient of the decomposition image of the $j$th layer; $d^{\mathrm{v}}_{j+1}, d^{\mathrm{h}}_{j+1}, d^{\mathrm{d}}_{j+1}$ represent the HF wavelet coefficient in the vertical, horizontal and diagonal directions, respectively; $p(k-2m), p(l-2n)$ mean carrying on the low-pass filter and then sampling in the directions of $y, x$, respectively; $q(k-2m), q(l-2n)$ mean carrying on the high-pass filter and then sampling in the directions of $y, x$, respectively; $p(m-2k), p(n-2l)$ mean carrying on interpolation and then low-pass filtering; $q(m-2k), q(n-2l)$ mean carrying on interpolation and then high-pass filtering.

$H_r$ and $H_c$ represent the coefficient matrix of the mirror-image conjugate filter $H$, which has an effect on the rows and columns of array $\{C_{k,l}\}_{k,l\in Z^2}$, respectively, $G_r$ and $G_c$ represent the coefficient matrix of the mirror-image conjugate filter $G$, which has an effect on the rows and columns of array $\{C_{k,l}\}_{k,l\in Z^2}$, respectively, so that we can have the wavelet decomposition algorithm of a two-dimensional image in a matrix form shown as follows:

$$
\begin{cases}
C_{j+1} = H_r H_c C_j \\
D^{v}_{j+1} = H_r G_c C_j \\
D^{h}_{j+1} = G_r H_c C_j \\
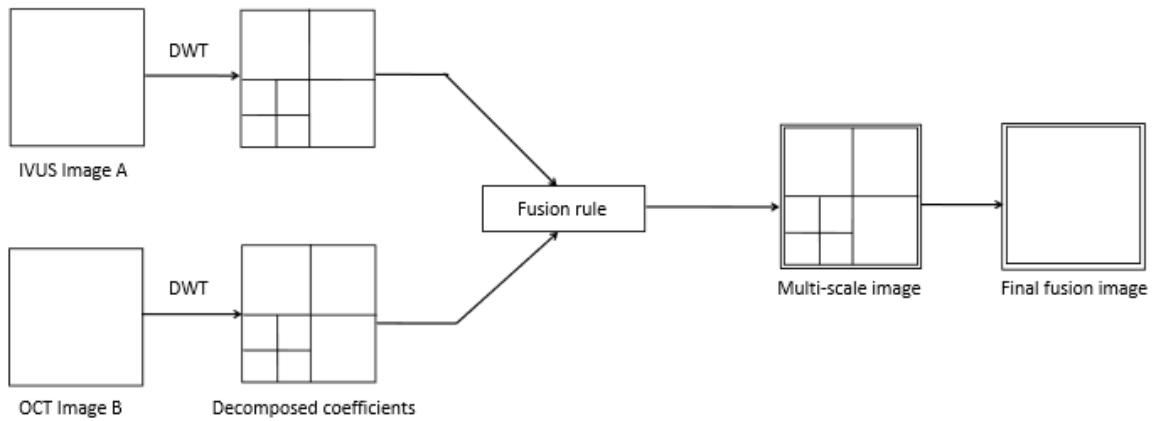D^{d}_{j+1} = G_r G_c C_j
\end{cases}
\tag{8}
$$

**FIGURE 4.** Block diagram of the proposed wavelet image fusion approach.
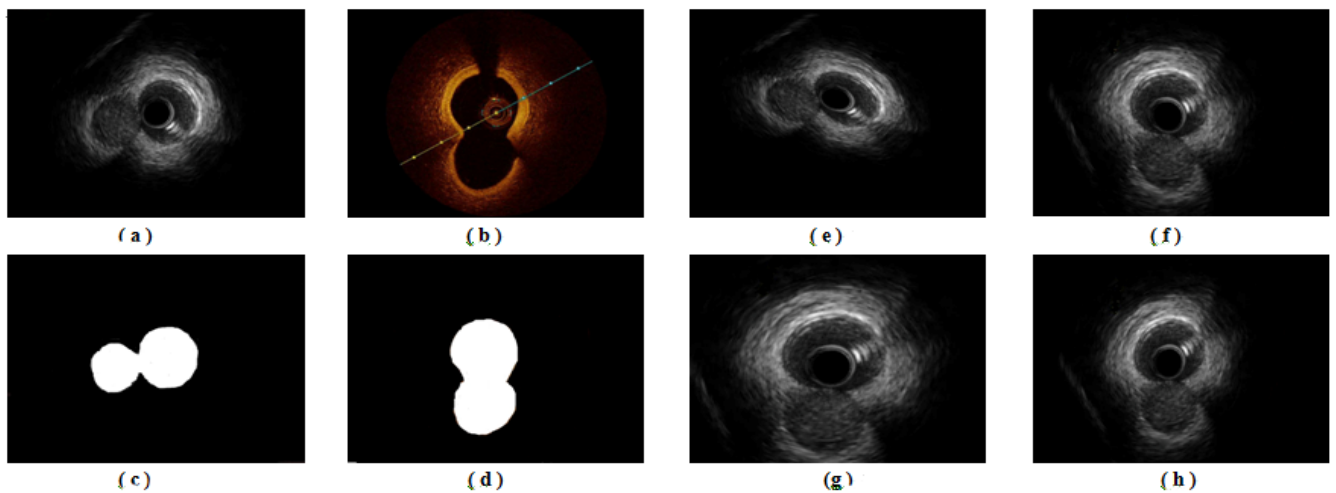
Set-1



**FIGURE 5.** Comparison of registration images with side branch. (a) IVUS original image, (b) OCT original image, (c) IVUS contour image, (d) OCT contour image, (e) registration image based on gray mutual information only, (f) registration image based on feature points only, (g) registration image based on both feature points and gray mutual information, (h) registration image based on contour, feature points and gray mutual information.

where $j = 0, 1, \ldots, J$. And the two-dimensional Mallet reconstruction algorithm is given by

$$C_j = H_r H_c C_{j+1} + H_r G_c D_{j+1}^v + G_r H_c D_{j+1}^h + G_r G_c D_{j+1}^d \tag{9}$$

Among them, $j = J, \ldots, 1, 0. C_j$ and $C_{j+1}$ represent the LF wavelet coefficient of the decomposition image of the $j + 1$th layer; $D_{j+1}^v, D_{j+1}^h, D_{j+1}^d$ are the HF wavelet coefficients in the vertical, horizontal and diagonal directions, respectively. LF components can reflect the approximate and average characteristics of the images, concentrate most of the energy of the image, and express the information of the whole overall outlines as well. In contrast, HF components reflect the information of mutation of the image, e.g., edges and area boundaries [11].

## III. RESULTS AND DISCUSSION

The framework was implemented on the platform of MATLAB 2016a and related tool-boxes (MathWorks,

Natick, MA, USA) together with in-house developed Python modules. The IVOCT and IVUS images were obtained from the Department of Cardiology, Shanghai Tongji Hospital of Tongji University, Shanghai, China. OCT images were acquired using the commercial C7-XR Fourier-Domain OCT system (St. Jude Medical, St. Paul, MN, USA) with a C7 Dragonfly catheter (St. Jude Medical). The experiments are conducted on two pairs of source images to verify the effectiveness of the proposed method on various sources of images. The images are classified as having stent and side branches.

### A. SUBJECTIVE EVALUATIONS OF EXPERIMENTAL RESULTS

Two sets of images for comparison are shown in Fig. 5 and Fig. 6. Fig. 7 and Fig. 8 show the result of RMSE contour images after registration. And (a) and (b) represent the IVUS contour image as a registration image and the OCT contour image as a reference image, respectively. It can be seen that
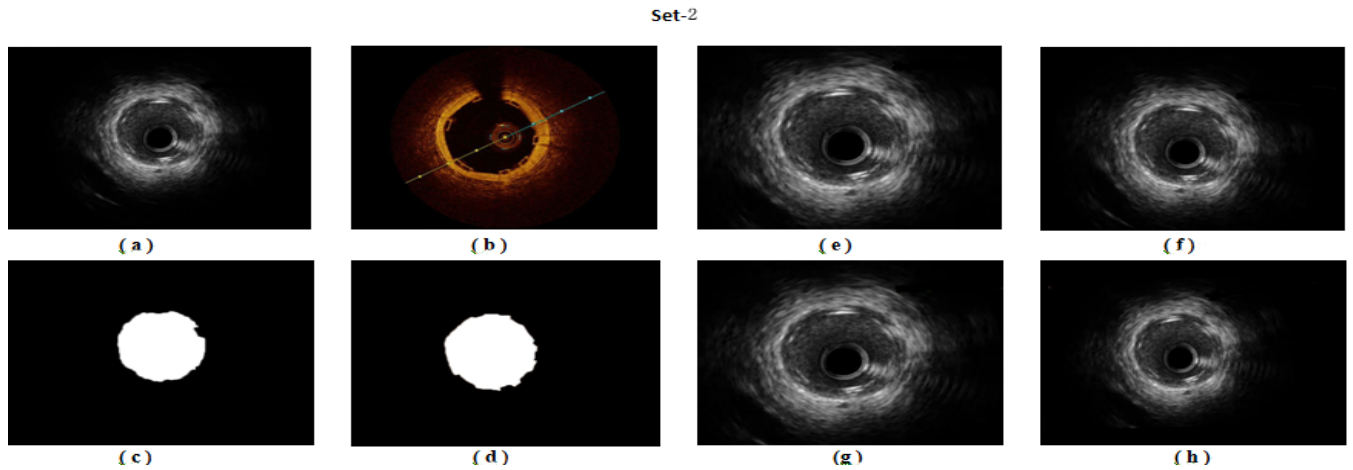
**Set-2**



**FIGURE 6.** Comparison of registration images with a stent. (a) IVUS original image, (b) OCT original image, (c) IVUS contour image, (d) OCT contour image, (e) registration image based on gray mutual information only, (f) registration image based on feature points only, (g) registration image based on both feature points and gray mutual information, (h) registration image based on contour, feature points and gray mutual information.
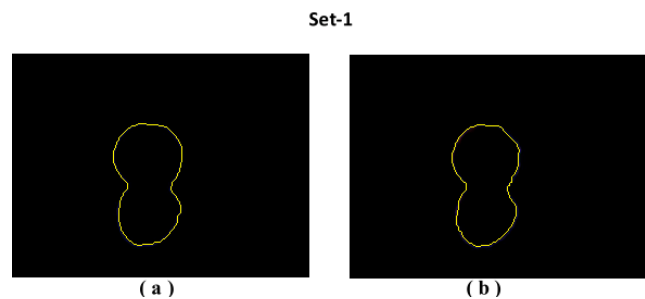


**FIGURE 7.** RMSE contour images with a side branch of (a) OCT and (b) IVUS.

**FIGURE 8.** RMSE contour images with a stent of (a) OCT and (b) IVUS.

image registration based on feature points or gray mutual information has limitations of image precision. A coarse-to-fine registration based on the combination of contour, gray mutual information and feature points is needed.

To evaluate the performance of the proposed approach for image fusion, a variety of types of wavelet bases are firstly taken into account, which includes haar, db8, sym8, coif5, bior2.4, rbio2.4 and dmey. As shown in Fig. 9, the haar-based fusion image is clearer than the others. The experimental result of various decomposition levels is shown in Fig. 10. Compared with the effectiveness of levels from 2 to 9, the decomposition level at 4 starts showing promising quality. Several methods are employed in the comparison including IHS, PCA, weighted average fusion rule and wavelet transformation. As shown in Fig. 11 to 12, in contrast to the IVUS original image, wavelet fusion presents an accurate image and contains more information. A series of experimental results conducted in this study demonstrated that the best performance was obtained by the wavelet fusion of haar-base and decomposition level at 4.

### B. OBJECTIVE EVALUATIONS OF THE EXPERIMENTAL RESULTS

Two hundred original IVUS and OCT images from Shanghai Tongji Hospital are used in the experiment on an
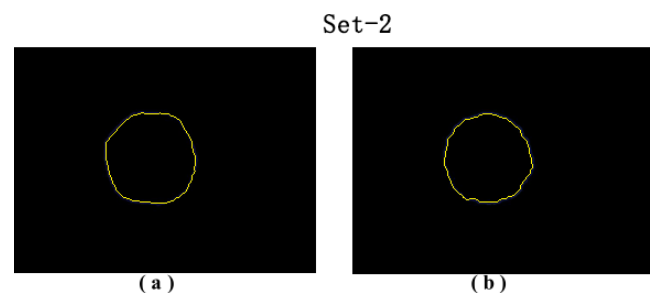
analytical basis. For quantitative evaluation of the performance of the proposed approach, objective evaluations of the images are given as follows.

### 1) ROOT MEAN SQUARE ERROR (RMSE)

The root mean square error is the arithmetic square root of the mean square error (MSE) as defined as

$$RMSE = \sqrt{(x'-x)^2 + (y'-y)^2} \qquad (10)$$

where $(x, y)$ and $(x', y')$ are the control points of the standard image and test image, respectively. The lower the value of MSE, the better is the fused result.

### 2) STANDARD DEVIATION (SD)

The standard deviation is used to describe the contrast of the fused image.

$$\sigma = \sqrt{\sum_{i=1}^{M}\sum_{j=1}^{N}(Z(x_i, y_j) - \bar{Z})^2/(M \times N)} \qquad (11)$$

where $Z(x_i, y_j)$ is the pixel value of the fused image and $\bar{Z}$ represents the mean value.

The SD reflects the discrete image gray-scale relative to the mean value of gray-scale.
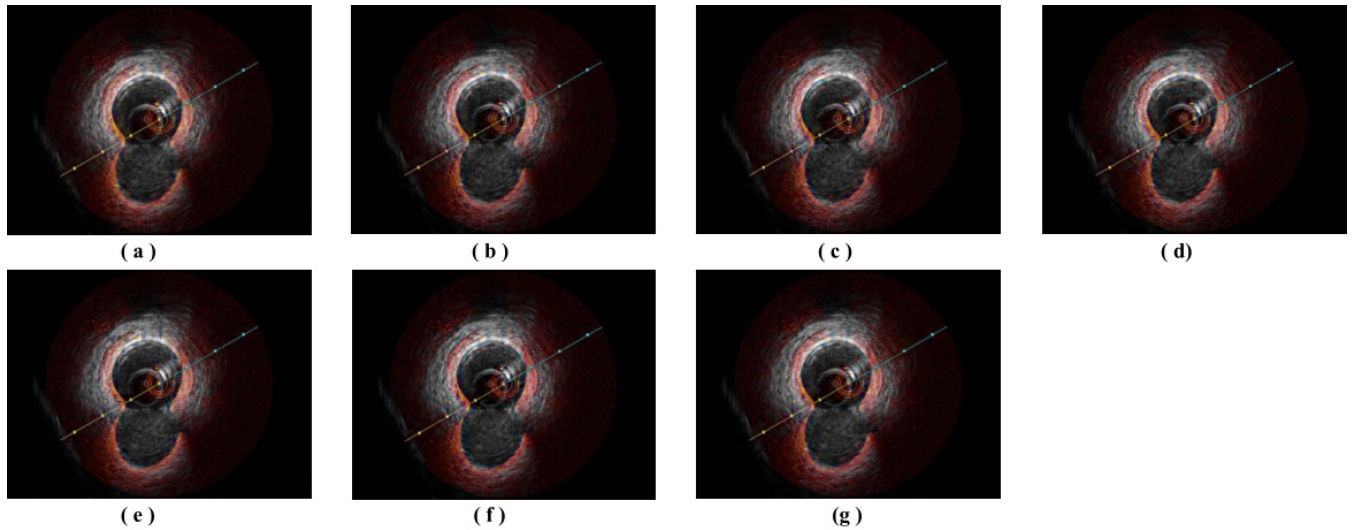
**FIGURE 9.** Comparison of the fused image using different wavelets (a) bior2.4, (b) coif5, (c) db8, (d) dmey, (e) haar, (f) rbio2.4, (g) sym8.
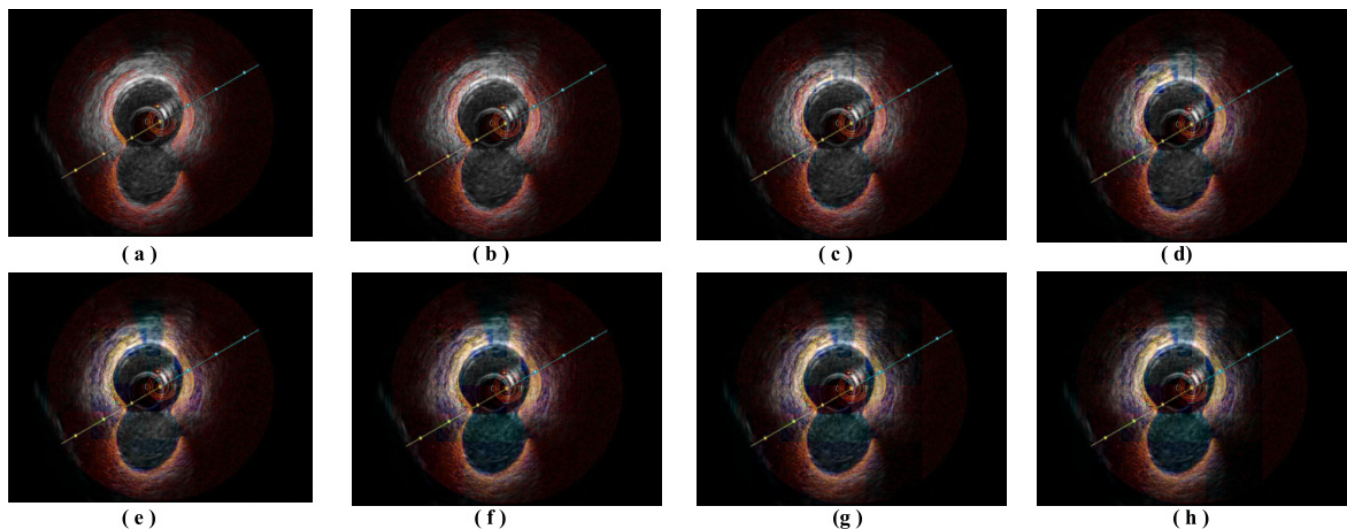


**FIGURE 10.** Comparison of the fused image using different decomposition levels. (a) to (h) represent the decomposition levels from 2 to 9, respectively.

### 3) INFORMATION ENTROPY (E)

The information entropy is defined as

$$E = -\sum_{i=0}^{L-1} p_i \log_2 p_i \tag{12}$$

where L is the image gray-scale and $P_i$ represents the proportion of the pixel of gray value $i$ in the whole pixels. A higher value of entropy indicates a greater amount of information in the fused image.

### 4) MEAN GRADIENT ($\bar{G}$)

The mean Gradient sensitively responded to the ability of the image to represent the contrast of tiny details.

$$\bar{G} = \frac{1}{(M-1)(N-1)}$$
$$\times \sum_{i=1}^{M-1}\sum_{j=1}^{N-1} \sqrt{((\frac{\partial Z(x_i, y_j)}{\partial x_i})^2 + (\frac{\partial Z(x_i, y_j)}{\partial y_i})^2)/2} \tag{13}$$

The $\bar{G}$ is used to evaluate the degree of fuzziness in the image. The higher the value of the mean gradient, the clearer the image is.

### 5) SPATIAL FREQUENCY (SF)

The spatial frequency is the measure of the overall activity in an image. For an image with gray value $Z(x_i, y_j)$ at position $(x_i, y_j)$, the spatial frequency is given by the equation

$$SF = \sqrt{RF^2 + CF^2} \tag{14}$$

where the row frequency is

$$RF = \sqrt{\frac{1}{M \times N} \sum_{i=1}^{M}\sum_{j=2}^{N} [Z(x_i, y_j) - Z(x_i, y_{j-1})]^2} \tag{15}$$
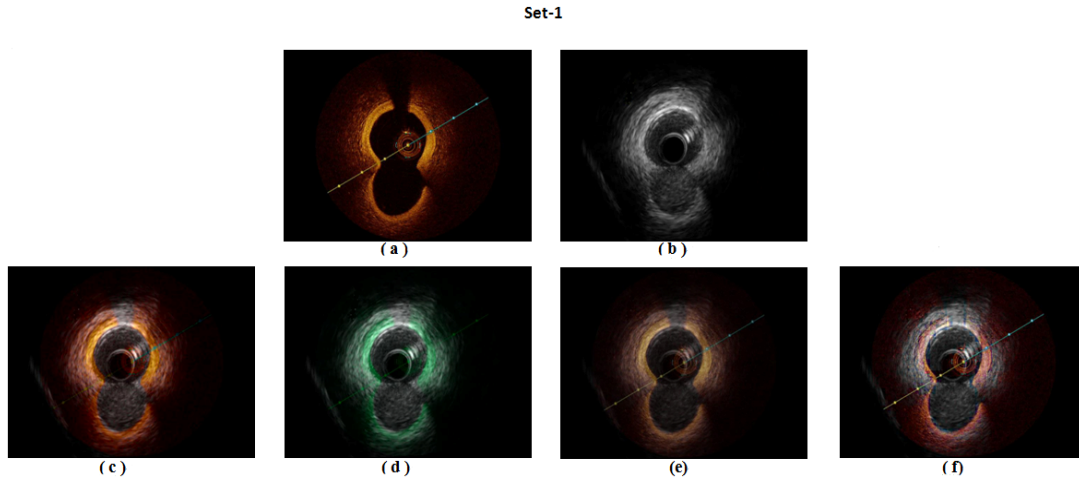
Set-1



**FIGURE 11.** Comparison of the fusion images with side branches. (a) Original OCT image, (b) IVUS registered image, (c) IHS fusion image, (d) PCA fusion image, (e) weighted fusion image, (f) wavelet fusion image.

Set-2



**FIGURE 12.** Comparison of the fusion images with a stent. (a) Original OCT image, (b) IVUS registered image, (c) IHS fusion image, (d) PCA fusion image, (e) weighted fusion image, (f) wavelet fusion image.
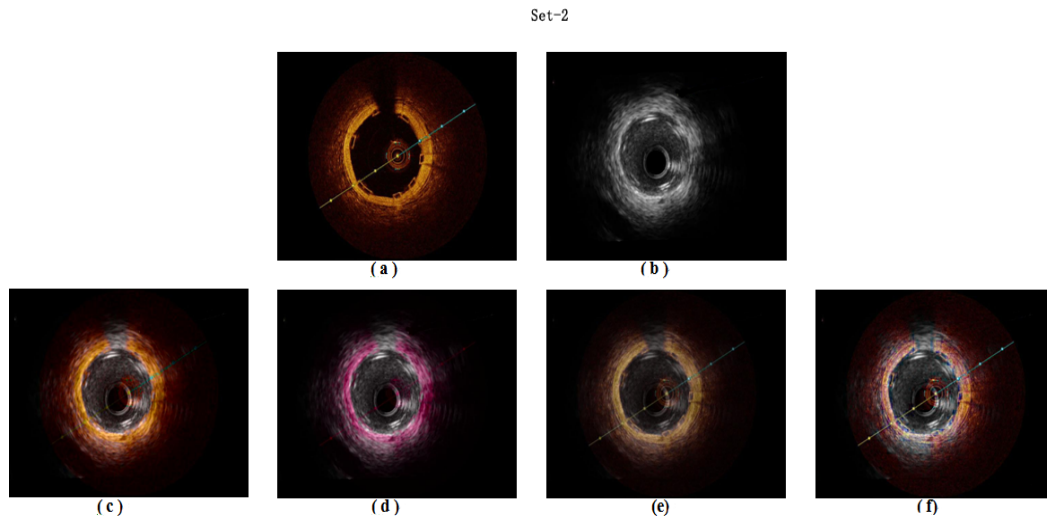
and the column frequency is

$$CF = \sqrt{\frac{1}{M \times N} \sum_{i=2}^{M} \sum_{j=1}^{N} [Z(x_i, y_j) - Z(x_{i-1}, y_j)]^2} \quad (16)$$

The higher the value of the frequency, the better is the image quality.

### 6) CORRELATION COEFFICIENT ($\rho_{FA}$)
The correlation coefficient is expressed as follows:

$$\rho_{FA} = \frac{\sum_{i=1}^{M} \sum_{j=1}^{N} [F(x_i, y_i) - \bar{f}][A(x_i, y_i) - \bar{a}]}{\sqrt{\sum_{i=1}^{M} \sum_{j=1}^{N} [F(x_i, y_i) - \bar{f}]^2 [A(x_i, y_i) - \bar{a}]^2}} \quad (17)$$

where $\bar{f}$ and $\bar{a}$ are the mean value of the fused image and the original image, respectively.

A higher value of $\rho_{FA}$ represents a better fusion result. The lower the value of MSE, the better is the fusion result.

The value of RMSE is 1.3979 for the data of Fig. 7 and 0.9201 for Fig. 8. The result demonstrates the effectiveness of the proposed method of coarse-to-fine registration. The results of using various wavelet bases are shown in Table 1 in which the best results are labeled in bold. It is shown that although the bior2.4-based fusion image has higher values of information entropy, standard deviation, average correlation coefficient and correlation coefficient of IVUS, the haar-base performs well in spatial frequency, mean gradient and correlation coefficient of OCT in contrast. It indicates that using the haar base for image fusion can offer a more desirable outcome, as information of individual images such as lines, curves, edges, and boundaries can be retained in a

**TABLE 1.** Comparison results for differentt wavelet bases.

| Wavelet bases | E | SF | σ | G | ρ |
|---|---|---|---|---|---|
| *haar* | 4.8533 | **17.0482** | 42.6475 | **6.2035** | 0.947 |
| *db8* | 4.8736 | 16.7774 | 42.4656 | 6.0373 | 0.94555 |
| *sym8* | 4.8762 | 16.8202 | 42.5345 | 6.132 | 0.9465 |
| *coif5* | 4.9006 | 16.8238 | 42.4327 | 6.0508 | 0.9462 |
| *bior2.4* | **4.9325** | 16.8345 | **42.9415** | 6.1321 | **0.9477** |
| *rbio2.4* | 4.843 | 16.9925 | 42.5183 | 6.1984 | 0.9448 |
| *dmey* | 4.9207 | 16.8076 | 42.3374 | 6.0255 | 0.94575 |

E = entropy, SF = spatial frequency, $\sigma$ = standard deviation, G = mean gradient, $\rho$ = correlation coefficient.

**TABLE 2.** Comparison results for differentt decomposition levels.

| Decomposition levels | E | SF | σ | G | ρ |
|---|---|---|---|---|---|
| *lev=2* | **4.9243** | 16.831 | 42.2961 | 6.0454 | 0.94605 |
| *lev=3* | 4.8955 | 16.9912 | 42.4312 | 6.1475 | 0.94615 |
| *lev=4* | 4.8533 | **17.0482** | 42.6475 | 6.2035 | 0.947 |
| *lev=5* | 4.8172 | 17.2083 | 42.9602 | 6.2661 | 0.94395 |
| *lev=6* | 4.7646 | 16.9711 | 43.6699 | 6.3758 | **0.9511** |
| *lev=7* | 4.7142 | 16.9274 | **44.0729** | 6.3236 | 0.95 |
| *lev=8* | 4.6456 | 16.8541 | 44.0486 | 6.6432 | 0.94995 |
| *lev=9* | 4.5921 | 16.7277 | 43.9279 | **6.7598** | 0.9489 |

E = entropy, SF = spatial frequency, $\sigma$ = standard deviation, G = mean gradient, $\rho$ = correlation coefficient.

**TABLE 3.** Comparison results for differentt fusion methods.

| Fusion methods | Entropy | | Spatial frequency | | Standard deviation | | Mean gradient | | Correlation coefficient | |
|---|---|---|---|---|---|---|---|---|---|---|
| | Set 1 | Set 2 | Set 1 | Set 2 | Set 1 | Set 2 | Set 1 | Set 2 | Set 1 | Set 2 |
| *IHS fusion* | 4.1366 | 3.9102 | 8.863 | 8.5226 | 34.1349 | 42.9322 | 2.9941 | 2.9554 | 0.7943 | 0.80255 |
| *Weighted fusion* | 4.5211 | 4.4132 | 8.4166 | 7.9908 | 26.1616 | 30.193 | 3.0863 | 3.0891 | **0.9582** | **0.95325** |
| *PCA fusion* | 4.3189 | 4.1317 | 8.7672 | 8.4578 | 31.1458 | 40.7097 | 3.1243 | 3.9149 | 0.7695 | 0.79525 |
| *Wavelet fusion* | **4.8533** | **4.7785** | **17.0482** | **16.105** | **37.6799** | **44.1765** | **6.2035** | **6.1647** | 0.947 | 0.9386 |

Set-1 is images with side branch, and Set-2 is images with stent.

better way. Table 2 shows the results obtained at various decomposition levels where the best results are marked in bold. It shows that the decomposition level at 2 produces good quality in information entropy and correlation coefficient of IVUS, while the decomposition level at 4 does prominently well in spatial frequency. Considering the standard deviation and correlation coefficient of OCT, the decomposition level at 7 achieves the best result. Moreover, the decomposition levels at 6 and 9 are better than others regarding the average correlation coefficient and mean gradient, respectively. The comparison experiments show that the wavelet decomposition level for haar-base image fusion of 4 levels is a promising solution. It can obtain a clearer image that contains more visual information. Table 3 shows the comparison results among a variety of fusion methods. As shown in Table 3 in

which the best results are labeled in bold, although weighted fusion performs well in the average correlation coefficient, wavelet fusion performs better than the other methods in information entropy, spatial frequency, standard deviation and mean gradient. It ensures that there is no information loss and redundant information of signal in the fusion process. Both the subjective or objective evaluation demonstrate the performance of the proposed framework that can get better registered performance and improved fusion effectiveness.

## C. DISCUSSION
In the proposed framework, feature-based registration extracts the core characteristics of an image and greatly compresses the information quantity of images as well. The analysis of our work shows that the precision of image features

registration based on contour or feature points is lower than gray registration. However, only using gray registration is unfit for the images under processing. In contrast, the combination of features registration and gray mutual information registration provides better performance in both precision and computational stability so that it can be widely used in most circumstances. In the process of image fusion, experiments are conducted to determine the appropriate types of wavelet base, the associated decomposition level and the use of the fusion algorithm. Considering a variety of performance measurements including the standard deviation, information entropy, mean gradient, spatial frequency and correlation coefficient, this study stated that the use of the wavelet fusion of haar-base at a decomposition level of 4 achieves the most promising performance.

The framework presented in this paper has a few improvements in the future. The selection of feature points has a direct effect on the image quality. In our work, the feature points are obtained through automatic detection and followed by manual pair matching. A fully automatic procedure for optimal pair matching will further improve the accuracy. In the step of fine-registration, the quality of the contour images we extract can also be considered, which probably influences the registration accuracy based on gray mutual information.

## IV. CONCLUSION

In this paper, a new framework for the fusion of intravascular ultrasound and optical coherence tomography images is proposed. It reinforces the details of atherosclerosis by fusing co-registered IVUS and IV-OCT images. The coarse-registration was processed based on feature points such as stent struts and side branches points. The next fine-registration is executed based on mutual information. Their cascading is feasible, and the experimental results show its promising performance. Moreover, compared to other fusion algorithms, the wavelet-based fusion method shows its best flexibility and high performance. To demonstrate the robustness of the proposed framework, both the subjective evaluation and objective evaluation were performed. The qualitative and quantitative experiments show the effectiveness of the proposed framework compared to the other registration and fusion algorithms. The fusion of intravascular ultrasound and optical coherence tomography clearly provides more comprehensive information for physicians in clinical practice. The physicians can understand the structure of atherosclerosis deeply and diagnose precisely. Future work will focus on the attempt to co-register whole IVUS and IV-OCT pullbacks of coronary arteries and improve the robustness of the registration.

## REFERENCES

[1] S. N. Blair, C. E. Barlow, R. S. Paffenbarger, Jr., and L. W. Gibbons, "Cardiovascular disease and all-cause mortality in men and women," *JAMA*, vol. 276, pp. 205–210, Feb. 1996.

[2] B. O. Isomaa *et al.*, "Cardiovascular morbidity and mortality associated with the metabolic syndrome," *Diabetes Care*, vol. 24, no. 4, pp. 683–689, 2001.

[3] M. Johanssona, H. Herlitzb, G. Jensenb, B. Rundqvist, and P. Friberga, "Increased cardiovascular mortality in hypertensive patients with renal artery stenosis. Relation to sympathetic activation, renal function and treatment regimens," *J. Hypertension*, vol. 17, no. 12, pp. 1743–1750, 1999.

[4] K. M. Anderson, P. M. Odell, P. W. F. Wilson, and W. B. Kannel, "Cardiovascular disease risk profiles," *Amer. Heart J.*, vol. 121, no. 1, pp. 293–298, 1991.

[5] A. Nair, B. D. Kuban, E. M. Tuzcu, P. Schoenhagen, S. E. Nissen, and D. G. Vince, "Coronary plaque classification with intravascular ultrasound radiofrequency data analysis," *Circulation*, vol. 106, no. 17, pp. 2200–2206, 2002.

[6] B. E. Bouma *et al.*, "Evaluation of intracoronary stenting by intravascular optical coherence tomography," *Heart*, vol. 89, no. 3, pp. 317–320, 2003.

[7] X. Li *et al.*, "Integrated IVUS-OCT imaging for atherosclerotic plaque characterization," *IEEE J. Sel. Topics Quantum Electron.*, vol. 20, no. 2, pp. 196–203, Mar. 2014.

[8] F. Alfonso *et al.*, "Combined use of optical coherence tomography and intravascular ultrasound imaging in patients undergoing coronary interventions for stent thrombosis," *Heart*, vol. 98, no. 16, pp. 1213–1220, 2012.

[9] B. H. Li *et al.*, "Hybrid intravascular ultrasound and optical coherence tomography catheter for imaging of coronary atherosclerosis," *Catheter Cardiovascular Intervent.*, vol. 81, no. 3, pp. 494–507, 2013.

[10] J. Yin *et al.*, "Novel combined miniature optical coherence tomography ultrasound probe for *in vivo* intravascular imaging," *J. Biomed. Opt.*, vol. 16, no. 6, p. 060505, 2011.

[11] Z. Sun and H. Hu, "Off-line fusion of intravascular ultrasound and optical coherence tomography images," *J. Med. Imag. Health Informat.*, vol. 7, no. 7, pp. 1531–1538, 2017.

[12] O. Pauly, G. Unal, and G. Slabaugh, "Semi-automatic matching of OCT and IVUS images for image fusion," presented at the Int. Soc. Opt. Eng., 2008.

[13] G. Unal, S. Lankton, S. Carlier, G. Slabuagh, and Y. Chen, "Fusion of IVUS and OCT through semi-automatic registration," in *Proc. CVII-MICCAI*, 2006, pp. 163–170.

[14] D. S. Molony, L. H. Timmins, E. Rasoul-Arzrumly, H. Samady, and D. P. Giddens, "Evaluation of a framework for the co-registration of intravascular ultrasound and optical coherence tomography coronary artery pullbacks," *J. Biomech.*, vol. 49, no. 16, pp. 4048–4056, 2016.

[15] J. P. W. Pluim, J. B. A. Maintz, and M. A. Viergever, "Mutual-information-based registration of medical images: A survey," *IEEE Trans. Med. Imag.*, vol. 22, no. 8, pp. 986–1004, Aug. 2003.

[16] G. Pajares and J. M. de la Cruz, "A wavelet-based image fusion tutorial," *Pattern Recognit.*, vol. 37, no. 9, pp. 1855–1872, 2004.

[17] M. Haddadpour, S. Daneshvar, and H. Seyedarabi, "PET and MRI image fusion based on combination of 2-D Hilbert transform and IHS method," *Biomed. J.*, vol. 40, no. 4, pp. 219–225, 2017.

[18] C. He, Q. Liu, H. Li, and H. Wang, "Multimodal medical image fusion based on IHS and PCA," *Proc. Eng.*, vol. 7, pp. 280–285, Jan. 2010.

[19] S. Cheng, J. He, and Z. Lv, "Medical image of PET/CT weighted fusion based on wavelet transform," presented at the ICBBE, 2008.

[20] F. P. M. Oliveira and J. M. R. S. Tavares, "Medical image registration: A review," *Comput. Methods Biomech. Biomed. Eng.*, vol. 17, no. 2, pp. 73–93, 2014.

[21] L. S. Athanasiou, F. Rikhtegar, and M. Z. Galon, "Fully automated lumen segmentation of intracoronary optical coherence tomography images," presented at the Int. Soc. Opt. Eng., 2016.

[22] A. Wang, J. Eggermont, N. Dekker, P. J. H. de Koning, J. H. C. Reiber, and J. Dijkstra, "3D assessment of stent cell size and side branch access in intravascular optical coherence tomographic pullback runs," *Comput. Med. Imag. Graph.*, vol. 38, no. 2, pp. 113–122, 2014.

[23] C. Huang, C. Wang, J. Tong, L. Zhang, F. Chen, and Y. Hao, "Automatic quantitative analysis of bioresorbable vascular scaffold struts in optical coherence tomography images using region growing," *J. Med. Imag. Health Inf.*, vol. 8, no. 1, pp. 98–104, 2018.

[24] D. Rotger, P. Radeva, and N. Bruining, "Automatic detection of bioabsorbable coronary stents in IVUS images using a cascade of classifiers," *IEEE Trans. Inf. Technol. Biomed.*, vol. 14, no. 2, pp. 535–537, Mar. 2010.

[25] H. Chui, L. Win, R. Schultz, J. S. Duncan, and A. Rangarajan, "A unified non-rigid feature registration method for brain mapping," *Med. Image Anal.*, vol. 7, no. 2, pp. 113–130, 2003.

**CHENXI HUANG** received the B.Sc. degree in computer science from Tongji University, Shanghai, China, in 2015, where he is currently pursuing the Ph.D. degree. His research interests include image processing, image reconstruction, data fusion, 3-D visualization, and machine learning.
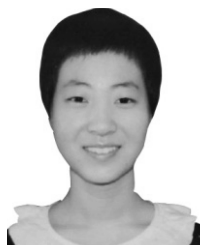
**YUAN XIE** is currently pursuing the B.Sc. degree with Tongji University, Shanghai, China. His research interests include image processing, reconstruction, and 3-D visualization.

**YISHA LAN** is currently pursuing the B.Sc. degree with Tongji University, Shanghai, China. Her research interests include image processing, reconstruction, and 3-D visualization.

**YONGTAO HAO** received the Ph.D. degree in mechanical engineering from Shanghai Jiao Tong University. He is currently a Professor with the College of Electronics and Information Engineering, Tongji University, and a Senior Member of Council for Chinese Mechanical Engineering Society. He has authored 40 articles, and holds six patents. His research interests include intelligent design, machine learning, data mining, Industry 4.0, integrated knowledge, and virtual reality.

**FEI CHEN** received the M.D. and Ph.D. degrees from the Medical College, Zhejiang University, Zhejiang, China. He is currently a Fellow Doctor with Tongji Hospital, Tongji University, Shanghai. His research interests include the pathophysiological proceeding of atherosclerosis, interventional treatment of CHD, image reconstruction of coronary stent, and 3-D visualization of coronary stent.

**YONGQIANG CHENG** is currently a Lecturer with the School of Engineering and Computer Science, University of Hull, U.K. His research interest includes digital healthcare technologies, embedded systems, control theory and applications, artificial intelligence, and data mining.

**YONGHONG PENG** (M'02) is currently a Professor of data science (Chair) and the Head of Data Science Research with the University of Sunderland, U.K. His research areas include data science, machine learning, data mining, and artificial intelligence. He is a Founding Member of the Technical Committee on Big Data of *IEEE Communications Magazine* and an advisory board member for the IEEE Special Interest Group on big data for cyber security and privacy. He is the Chair for the Big Data Task Force, and a member of Data Mining and Big Data Analytics Technical Committee of the IEEE Computational Intelligence Society. He is an Associate Editor for the IEEE Transaction on Big Data, and an Academic Editor of *PeerJ* and *PeerJ Computer Science*.

• • •